



# A study on Sb doping in lead tungstate crystals

Xiangdong Qu<sup>a</sup>, Liyuan Zhang<sup>a</sup>, Ren-Yuan Zhu<sup>a,\*</sup>, Qun Deng<sup>b</sup>,  
Jingying Liao<sup>b</sup>, Zhiwen Yin<sup>b</sup>

<sup>a</sup> *HEP, California Institute of Technology, 256-48 Pasadena, CA 91125, USA*

<sup>b</sup> *Shanghai Institute of Ceramics, Shanghai, 200050, People's Republic of China*

Received 18 October 2000; received in revised form 23 November 2000; accepted 28 November 2000

## Abstract

In this paper, we present results of a study on Sb doping in lead tungstate crystals. The crystal growth by modified Bridgman method is described. Result of trace analysis on raw materials and crystals is presented. The segregation coefficient of Sb ions in lead tungstate crystals was determined. The scintillation emission and longitudinal transmittance spectra, light output, decay kinetics and radiation damage were measured. It is found that Sb doping alone is not sufficient to produce radiation hard lead tungstate crystals, and post growth oxygen compensation is required. © 2001 Elsevier Science B.V. All rights reserved.

*PACS:* 81.10; 81.40

*Keywords:* Modified Bridgman method; Crystal growth; lead tungstate; Doping; Radiation hardness

## 1. Introduction

Because of its high density and fast decay time, lead tungstate ( $\text{PbWO}_4$ ) crystal was chosen by the compact muon solenoid (CMS) experiment to construct a precision electromagnetic calorimeter (ECAL) at the large hadronic collider (LHC) [1]. Good radiation resistance, however, is required for the use of  $\text{PbWO}_4$  crystals in the CMS ECAL since the radiation level at LHC is expected to be around 15 rad/h in barrel and up to 500 rad/h at endcaps [2]. An effort has been made in the last five years at Shanghai institute of ceramics (SIC) to develop radiation hard  $\text{PbWO}_4$  crystals for applications in severe radiation environment, such as

the CMS experiment. Our previous studies have led to an assumption that the radiation damage in  $\text{PbWO}_4$  crystals is caused by host structure defects, such as oxygen or lead vacancies [3,4], which introduce local charge imbalance and trap electrons or holes and thus form color centers.

One approach to reduce density of host structure defects is to optimize the stoichiometric ratio between two oxide raw materials and make a stringent control during crystal growth. This approach was attempted by SIC as well as other groups [5,6]. It is found that this optimization alone is not sufficient to reach required radiation hardness for the CMS. Various approaches to suppress or compensate the remaining defects were taken. Oxygen compensation, referring to post growth annealing at high temperature in an oxygen rich atmosphere, was found effective at SIC [7], indicating main mechanism of radiation

\*Corresponding author. Tel.: +1-626-395-6661; fax: +1-626-795-3951.

*E-mail address:* zhu@hep.caltech.edu (R.-Y. Zhu).

damage in  $\text{PbWO}_4$  is oxygen vacancies, i.e. electron centers.

Doping during crystal growth is another approach to either artificially introduce local charge imbalance and thus compensate structure defects or function as scavenger to further eliminate unwanted impurities. In development of BGO crystals for the L3 experiment, Eu doping was used at SIC to improve its radiation resistance [8]. In development of  $\text{CsI(Tl)}$  crystals for the *BaBar* and BELLE experiments, a special scavenger was used at SIC to remove oxygen contamination [7]. Pentavalent (Nb) doping in  $\text{PbWO}_4$  was first reported by Lecoq et al. to be effective in improving transmittance at 100 ppm level [9]. Trivalent (La) doping was first reported by Kobayashi et al. to be effective in improving both transmittance [10] and radiation hardness [11]. Consequent studies on doping with various ions, such as La, Lu, Gd, Y and Nb, at optimized level were reported to be effective in improving transmittance as well as radiation hardness [12,13].

Along the same direction, doping was extensively studied at SIC. While a complete summary of this study will be given elsewhere, this paper discusses doping with Sb. Since Sb ions exist in both trivalent and pentavalent forms it was hoped that both electron and hole centers may be compensated by Sb doping. This paper presents growth of doped crystals by modified Bridgman method and result of their optical properties and radiation resistance. It is found that Sb doping alone is not sufficient to produce radiation hard  $\text{PbWO}_4$  crystals, and post growth oxygen compensation is required.

## 2. Growth of Sb doped $\text{PbWO}_4$ crystals

$\text{PbWO}_4$  crystals are grown by modified Bridgman technique in Shanghai Institute of Ceramics, Shanghai, China. Raw materials of high purity, PbO and  $\text{WO}_3$ , are produced in Shanghai, and are mixed in precise stoichiometric proportion of  $\text{PbWO}_4$  in an agate mortar. The mixture is first melted in a platinum crucible in air to ensure complete homogeneity. After heated to high temperature this melt is sintered into platinum

crucible to form polycrystalline  $\text{PbWO}_4$  grogs for crystal growth.

Fig. 1 shows a schematic of a crucible used at SIC for  $\text{PbWO}_4$  crystal growth by modified Bridgman method. Multi crucibles with individual computer controlled temperature profile are constructed in each furnace, allowing multi pulling in one furnace. The layout of the furnace and its temperature profile can be found in Ref. [14]. Furnaces of this kind were early developed at SIC to grow BGO crystals for the L3 experiment at LEP, and were later successfully adapted to grow  $\text{CsI(Tl)}$  crystals for two B factories experiments *BaBar* and BELLE. The same technology is now used to grow  $\text{PbWO}_4$  crystals for the CMS.

The stability of temperature field in furnace is crucial for a successful growth of large size crystals. The temperature in these furnaces was monitored by Pt–Pt/Rh thermocouples and controlled by DWT-702 temperature controller. During crystal growth the variation of temperature is required to be less than  $0.5^\circ\text{C}$ , which stabilizes the crystal growth rate and reduces the density gradient in the diffusion layer of the solid–liquid

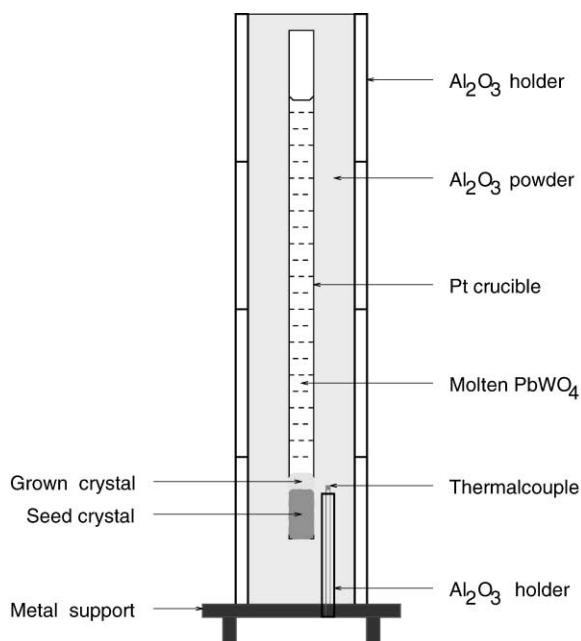


Fig. 1. A schematic showing a crucible used for  $\text{PbWO}_4$  crystal growth by modified Bridgman method at SIC.

interface so that the density of constitutional super-cooling defects is minimized.

Crystals were grown along the *c*-axis at SIC. Twenty eight crucibles of rectangular shape are constructed in every furnace for CMS PbWO<sub>4</sub> crystal growth. This shape of crucible makes efficient use of raw material since only a small fraction of ingot needs to be cut off to make final dimension. As-grown PbWO<sub>4</sub> crystals are transparent, colorless without visible defects, such as cracking, inclusions, scattering centers and growth striation.

### 2.1. Raw materials

Raw materials used to grow scintillation crystals are required to have high purity, preferable 5 N or 6 N. The high cost, however, prevents the use of material of extra high purity. Research is needed to find and selectively remove harmful impurities. Various material characterization means are available to determine trace elements in raw material as well as crystals. Among them glow discharge mass spectroscopy (GDMS) analysis is commonly used. It surveys 77 elements in a sample with precision of sub ppm level for metallic contamination.

Previous GDMS analysis revealed that cation, especially Mo, contamination is responsible for slow scintillation component in PbWO<sub>4</sub>, as reported early by Kobayashi et al. [15] and Zhu et al. [4]. Since Mo is naturally contaminated in WO<sub>3</sub>, special effort was made to reduce its contamination. After removing Mo and other cation contamination, PbWO<sub>4</sub> crystals produced at SIC have significantly reduced slow component.

Table 1 lists GDMS analysis result, in ppm weight (ppmw), of trace impurities in raw materials of different batches produced since 1998. The date when these raw materials were produced and the sum of the transition metals (TM): Sc, Ti, V, Cr, Mn, Fe, Co, Ni, Cu and Zn, and the sum of rare earth elements (RE): Ce, Pr, Nd, Eu, Sm, Gd, Tb, Dy, Ho, Er, Tm, Yb and Lu is also listed. The Mo contamination is found to be less than 1 ppm. This result of GDMS analysis shows that raw materials used at SIC have stable high purity.

### 2.2. Sb distribution in PbWO<sub>4</sub> crystals

Table 2 lists GDMS analysis result of some impurities (ppmw), except Sb, at positions *Z*(cm) from the top of ingot for some Sb-doped PbWO<sub>4</sub> samples grown by using raw materials listed in Table 1. The result shows that most trace elements are at the same level of those in raw materials, indicating no additional contamination in growth process.

Table 3 lists GDMS result of Sb concentration (ppmw) in ten Sb doped samples at positions *Z* × (cm) from the top of ingot. Also listed is initial Sb concentration (ppmw) in melt (Melt). The Sb distribution in PbWO<sub>4</sub> is not uniform with most Sb ions concentrated at the top end of ingots. The data in Table 3 are used to extract the segregation coefficient of Sb in PbWO<sub>4</sub>.

The segregation coefficient  $k_s$ , defined as the ratio of the dopant concentration in the bulk crystal ( $C_{\text{crystal}}$ ) to that in the melt ( $C_{\text{melt}}$ ), describes the ability of the dopant to be incorporated into the solid phase,

Table 1  
Result of GDMS analysis (ppmw) for raw materials

	Na	Mg	Al	Si	K	Ca	Mo	Sb	TM <sup>a</sup>	RE <sup>b</sup>	Date
PbO	0.08	0.01	0.7	0.15	0.15	<.05	0.01	<.05	0.5	<0.3	04/98
PbO	0.03	0.01	0.42	0.12	0.06	0.18	0.03	<.05	<0.3	<0.5	11/98
PbO	0.02	0.05	0.85	0.27	<.05	0.22	<.01	<.05	<0.4	<0.5	03/99
WO <sub>3</sub>	0.15	0.04	0.22	0.15	0.23	0.36	0.61	0.20	1.1	<0.2	04/98
WO <sub>3</sub>	0.07	0.01	0.22	0.25	0.32	0.11	0.61	<.05	<1.0	<0.5	11/98
WO <sub>3</sub>	0.07	<.01	0.30	0.25	0.11	<.07	0.20	<.05	<0.4	<0.3	03/99

<sup>a</sup> TM represents the sum of transition metals.

<sup>b</sup> RE represents the sum of rare earths.

Table 2  
Result of GDMS analysis (ppmw) for PbWO<sub>4</sub> crystal samples

ID	Z(cm)	Na	Mg	Al	Si	K	Ca	Mo	Sb	TM <sup>a</sup>	RE <sup>b</sup>
227	12	0.57	0.05	0.10	0.48	1.1	1.0	0.30	27	<0.9	<1.8
	22	0.05	0.04	0.26	0.31	0.16	0.30	0.51	18	<0.5	<1.0
275	4	1.2	<.01	0.04	0.07	0.1	0.12	0.25	110	<0.4	<0.7
	29	1.0	<.01	0.05	0.13	0.2	0.30	0.17	26	<0.3	<0.9
230	29	0.11	0.02	0.11	0.64	0.24	0.84	0.72	20	<0.2	<0.3
J16	—	0.73	0.02	0.21	0.26	2.5	1.3	0.92	89	<0.2	<0.3

<sup>a</sup>TM represents the sum of transition metals.

<sup>b</sup>RE represents the sum of rare earths.

Table 3  
Result of GDMS analysis of Sb concentration (ppmw) in PbWO<sub>4</sub> crystals

ID	227	234	268	275	285	286	295	325	332	338
Melt	401	134	294	214	294	241	241	214	161	268
Z	12/22	10/26	12/22	4/29	4/27.5	2/27.5	6/29.5	4/23	2.5/24	5/29
Sb	27/18	55/12	68/22	110/26	83/29	63/21	94/18	36/11	48/10	39/16

$$k_e = \frac{C_{\text{crystal}}}{C_{\text{melt}}} \quad (1)$$

Assuming a slow, steady state growth process, the distribution of dopant concentration in crystal can be expressed as

$$C_{\text{crystal}}(g) = k_e \frac{C_0 - \int_0^g C_{\text{crystal}}(t) dt}{1-g} \quad (2)$$

where  $C_0$  is the initial dopant concentration in the melt,  $g$  is the relative solidification coefficient, defined as the ratio of the volume of solidification part of the crystal to the whole volume of the crystal ingot. The solution of Eq. (2) is

$$C_{\text{crystal}} = k_e C_0 (1-g)^{k_e-1}. \quad (3)$$

Taking logarithm, Eq. (3) can be written as a linear equation:

$$\ln \frac{C_{\text{crystal}}}{C_0} = \ln k_e + (k_e - 1) \ln(1-g). \quad (4)$$

Fig. 2 shows a linear fit to the GDMS data. The numerical result of the effective segregation

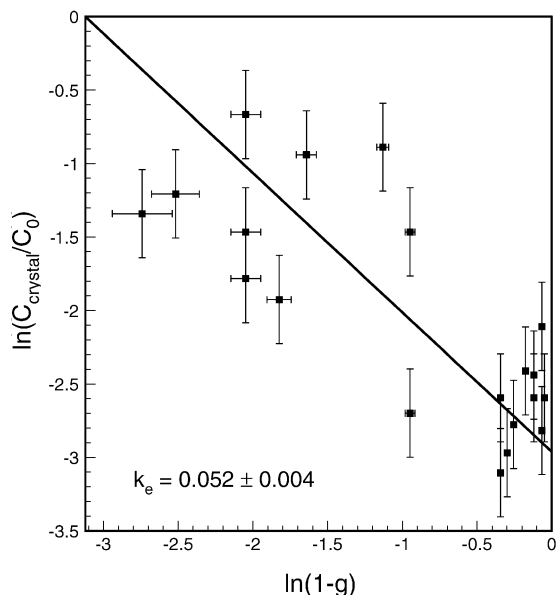


Fig. 2. A linear fit to the logarithm of Sb concentration in PbWO<sub>4</sub> crystals.

coefficient of Sb ions in  $\text{PbWO}_4$  crystals is found to be  $0.052 \pm 0.004$ , indicating only a small fraction of Sb ions would enter  $\text{PbWO}_4$  lattice.

### 3. Properties of Sb doped $\text{PbWO}_4$ crystals

Seven Sb doped  $\text{PbWO}_4$  samples, grown by using raw materials in Table 1, were studied. Table 4 lists their dimensions, date produced, Sb concentration in melt, post growth annealing condition and peak wavelengths of photo ( $\lambda_{\text{pho}}$ ) and radio ( $\lambda_{\text{rad}}$ ) luminescence.

All samples were grown at SIC by modified Bridgman method. While samples S078, AB49, J16 and 274 have a rectangular shape, 230 and 275 are full size samples with CMS tapered geometry. Samples were prepared in two ways, i.e. with (J16, 227, 230, 274, 275) and without (S078 and AB49) oxygen compensation. The oxygen compensation was carried out in conditions optimized for temperature, duration and partial pressure of the oxygen. These optimized conditions were determined by a systematic experiment on pairs of samples cut from different ingots to make sure they are adequate for all crystals.

The optical properties and light output of these samples are characterized at Caltech both before and after irradiation. All irradiation was carried out by using a  $^{60}\text{Co}$   $\gamma$ -ray source of 50 curie. During irradiation, samples were wrapped with Tyvek paper and aluminum foil, and were placed at a fixed distance to the source, so that entire body of the sample is under a defined dose rate.

Samples were under irradiation all the time, except when measurements were carried out, which typically lasted for less than 1 h. All measurements on the samples after irradiation were carried out in the dark to minimize optical bleaching effect. More detailed discussions on the equipment and techniques used for optical property and light output measurement can be found in reference [3].

#### 3.1. Photo and radio luminescence

Photo luminescence was measured by using a Hitachi F-4500 fluorescence spectrophotometer. A schematic of the measurement setup is shown in Fig. 3, where UV excitation light was shot to a bare surface of the sample and photo luminescence, without passing through sample, was measured by a photo multiplier tube (PMT) through a monochromator. The setup used to measure radio luminescence is shown in Fig. 4,

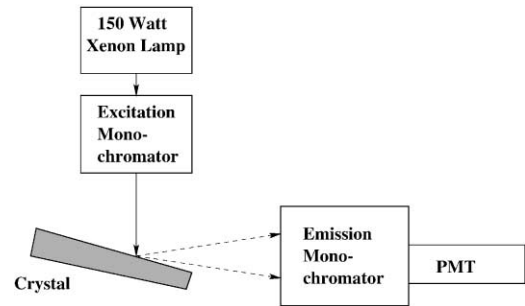


Fig. 3. A schematic of setup used to measure photo luminescence.

Table 4  
Sb doped  $\text{PbWO}_4$  samples<sup>a</sup>

ID	Dimension (cm)	Date	Melt (ppmw)	Annealing	$\lambda_{\text{pho}}$ (nm)	$\lambda_{\text{rad}}$ (nm)
S078	$2.4 \times 10.0 \times 2.4$	07/99	161	—	480	430
AB49	$2.2 \times 10.0 \times 2.2$	07/99	214	—	480	430
J16	$2.5 \times 10.5 \times 2.5$	05/98	268	$\text{O}_2$	510	—
227	$2.2 \times 13.3 \times 2.2$	11/98	401	$\text{O}_2$	510	—
230	$2.2 \times 23.0 \times 2.6$	11/98	268	$\text{O}_2$	510	—
274	$2.5 \times 21.0 \times 2.5$	10/98	268	$\text{O}_2$	510	450
275	$2.2 \times 23.0 \times 2.6$	10/98	214	$\text{O}_2$	510	—

<sup>a</sup>  $\text{O}_2$  represents high temperature annealing in  $\text{O}_2$ , i.e. oxygen compensation.

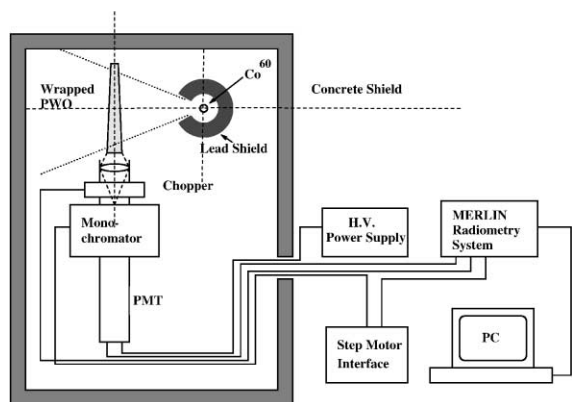


Fig. 4. A schematic of setup used to measure radio luminescence.

where whole body of a wrapped sample was irradiated by a  $^{60}\text{Co}$   $\gamma$ -ray source at a dose rate of about 1000 rad/h, and the radio luminescence, passing through sample, was focused, passed through a monochromator and measured by a PMT.

The peak wavelength of photo ( $\lambda_{\text{pho}}$ ) and radio ( $\lambda_{\text{rad}}$ ) luminescence is listed in Table 4. A comparison of photo (solid) and radio (dashed) luminescence spectra is shown in Figs. 5 and 6. These spectra were corrected for the wavelength dependence of light source intensity, monochromator grating efficiency and photo detector quantum efficiency. The vertical axis “Intensity” refers to photon numbers, and its scale is arbitrary.

It is interesting to note that the peak of photo luminescence of Sb doped samples is similar to that of undoped samples, while the peak of radio luminescence is similar to that of trivalent doped samples [16]. One also notices that the peak of radio luminescence is 50 to 60 nm blue shifted as compared to the photo luminescence. The origin of this blue shift is suspected due to that the UV photon is not energetic enough to excite the scintillation centers in Sb doped sample. This assumption was confirmed by an X-ray luminescence spectrum with a peak consistent with radio luminescence. One also notices that oxygen compensation has no effect on scintillation for Sb doped samples. Measurements by other group [17] show similar result.

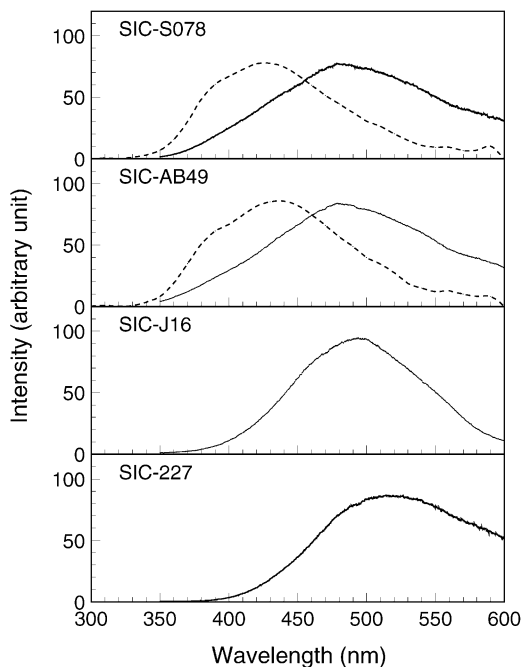


Fig. 5. Photo (solid) and radio (dashed) luminescence spectra for four small  $\text{PbWO}_4$  samples.

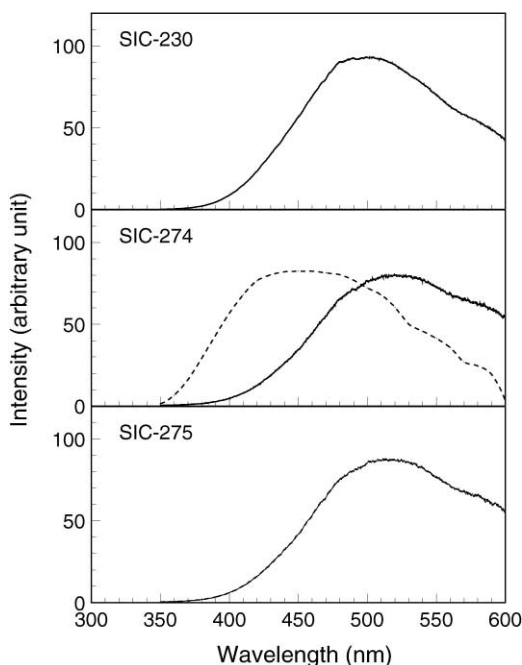


Fig. 6. Photo (solid) and radio (dashed) luminescence spectra for three full size  $\text{PbWO}_4$  samples.

### 3.2. Light output and decay kinetics

The scintillation light output and decay kinetics were measured using a Hamamatsu PMT R2059, which has a bialkali photo cathode and a quartz window. For the measurement of light output the large end of a sample was coupled to the PMT with Dow Corning 200 fluid, while all other faces of the sample were wrapped with Tyvek paper. A collimated  $^{137}\text{Cs}$  source was used to excite the sample. The  $\gamma$ -ray peak was obtained by a simple Gaussian fit, and was used to determine photoelectron numbers by using calibration of the single photoelectron peak.

Figs. 7 and 8 show light output as a function of the integrated gate width. The light output in these figures is in a unit of number of photoelectrons per MeV of energy deposition (p.e./MeV). The ratio of light output between 100 and 1000 ns is about 90%, as compared to typical 85% for undoped  $\text{PbWO}_4$  crystals. The trivalent doped  $\text{PbWO}_4$  sample, however, is faster. This ratio is typically

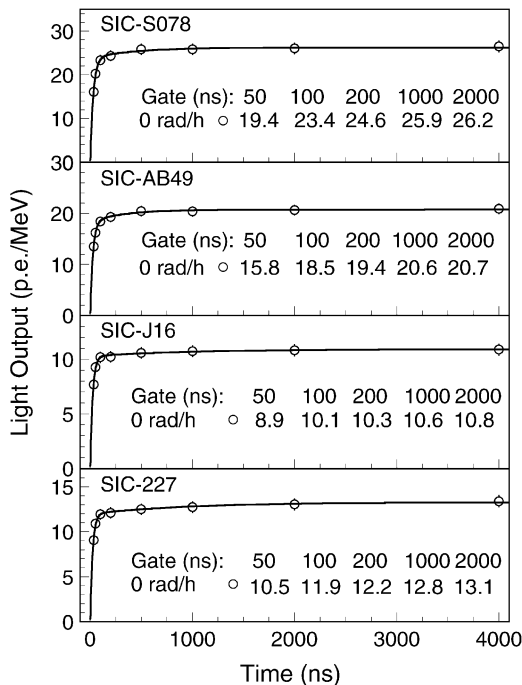


Fig. 7. Light output of four small size  $\text{PbWO}_4$  samples is shown as a function of integration time.

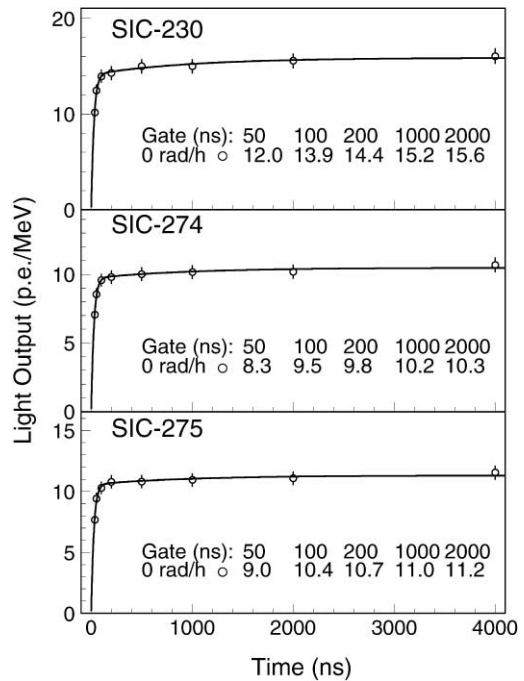


Fig. 8. Light output of three large size  $\text{PbWO}_4$  samples is shown as a function of integration time.

98% for Y doped samples. The oxygen compensation seems having no significant effect on decay kinetics. Sample S078 and AB49, which did not go through oxygen compensation, however, have significantly higher light output than other samples of similar size, which were prepared with oxygen compensation. The origin of this increase of light output is yet to be understood.

### 3.3. Longitudinal transmittance

Longitudinal transmittance was measured by using a Hitachi U-3210 UV/visible spectrophotometer with double beam, double monochromator and a large sample compartment equipped with a custom Halon coated integrating sphere. The systematic uncertainty in repeated measurements of transmittance was approximately 0.3%.

Fig. 9 shows the longitudinal transmittance as a function of wavelength measured before and after a series of irradiations for four small  $\text{PbWO}_4$

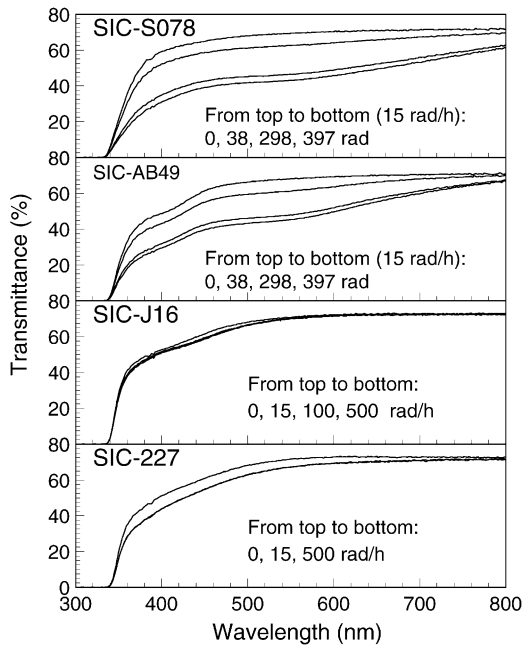


Fig. 9. Longitudinal transmittance is shown as a function of wavelength for four small  $\text{PbWO}_4$  samples before and after irradiation.

crystals. The curves in each plot in an order from the top to the bottom represent the transmittance before irradiation and that immediately after irradiation with dose or dose rate specified in the figure. For samples S078 and AB49, the irradiation was carried out at a dose rate of 15 rad/h with cumulated dosage of 38, 298 and 397 rad. The last two curves are close to each other, indicating that radiation damage in these two samples approach an equilibrium as explained in Section 3.4 below. It is clear that these two samples suffer from significant radiation damage. For samples J16 and 227, longitudinal transmittance was measured after these samples reached an equilibrium at dose rate of 15, 100 and 500 rad/h. Since samples S078 and AB49 were prepared without any annealing, while samples J16 and 227 were prepared with optimized oxygen compensation, this result indicates an improvement of radiation resistance for Sb doped samples with oxygen compensation.

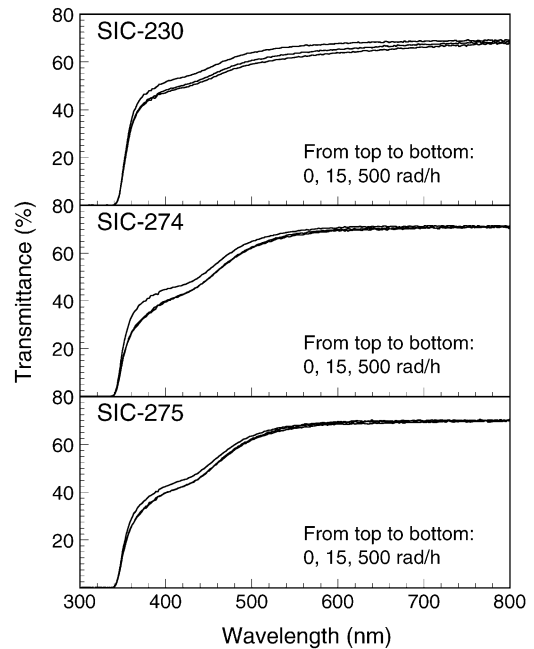


Fig. 10. Longitudinal transmittance is shown as a function of wavelength for three full size  $\text{PbWO}_4$  samples before and after irradiation.

Fig. 10 shows longitudinal transmittance of samples 230, 274 and 275, measured before irradiation and in equilibrium at dose rate of 15 and 500 rad/h. The small difference in transmittance before and after irradiations indicates that Sb doped samples after oxygen compensation are radiation hard. One also notices that these Sb doped samples suffer from preexisting color centers before irradiation. The nature of these centers is yet to be understood.

### 3.4. Radiation induced color centers

It is known that radiation induced color centers are created in  $\text{PbWO}_4$  crystals by irradiation, and may annihilate in room temperature. During irradiation, both annihilation and creation process coexist, the color center density reaches an equilibrium at a level depending on the dose rate applied. Assuming the annihilation speed of color center  $i$  is proportional to a constant  $a_i$  and its creation speed is proportional to a constant  $b_i$  and

the dose rate ( $R$ ), the differential variation of color center density when both processes coexist can be written as [7]

$$dD = \sum_{i=1}^n \{-a_i D_i + (D_i^{\text{all}} - D_i) b_i R\} dt, \quad (5)$$

where  $D_i$  is the density of the color center  $i$  in the crystal and the summation goes through all centers. The solution of Eq. (5) is

$$D = \sum_{i=1}^n \left\{ \frac{b_i R D_i^{\text{all}}}{a_i + b_i R} \left[ 1 - e^{-(a_i + b_i R)t} + D_i^0 e^{-(a_i + b_i R)t} \right] \right\}, \quad (6)$$

where  $D_i^{\text{all}}$  is the total density of the trap related to the center  $i$  and  $D_i^0$  is its initial density. The color center density in equilibrium ( $D_{\text{eq}}$ ) depends on the dose rate ( $R$ ) applied:

$$D_{\text{eq}} = \sum_{i=1}^n \frac{b_i R D_i^{\text{all}}}{a_i + b_i R}. \quad (7)$$

Figs. 11 and 12 show radiation induced color center density as function of photon energy for

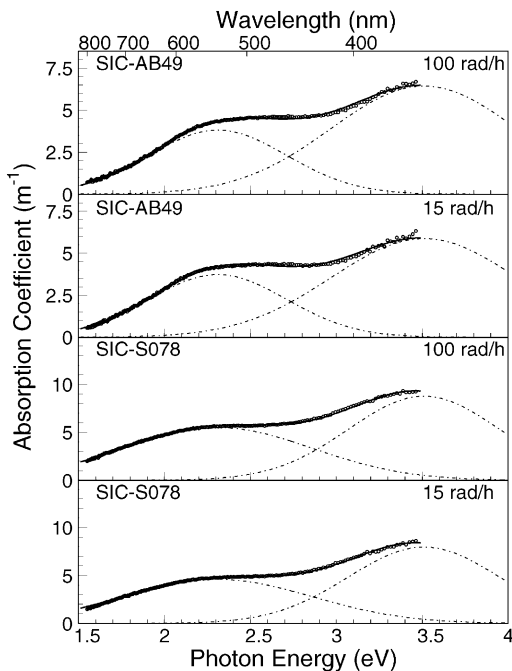


Fig. 11. Radiation induced color center density for samples AB49 and S078.

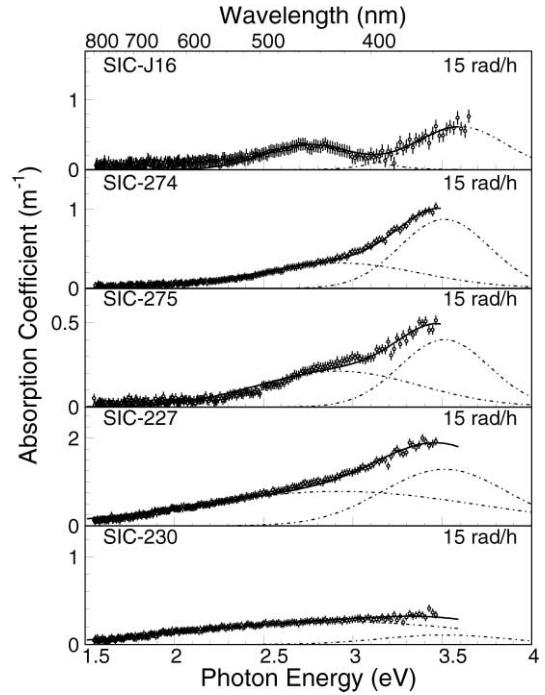


Fig. 12. Radiation induced color center density for J16, 274, 275, 227 and 230.

sample AB49 and S078 and J16, 274, 275, 227 and 230, respectively. The points with error bars are radiation induced color center density ( $D$ ), or absorption coefficient, measured in equilibrium under dose rates specified. They were calculated according to an equation

$$D = 1/LAL_{\text{equilibrium}} - 1/LAL_{\text{before}}. \quad (8)$$

where LAL is light attenuation length calculated by using longitudinal transmittance according to Eq. (1) of Ref. [3], and the subscript “equilibrium” and “before” refer to “in equilibrium” and “before irradiation” respectively. The radiation induced color center density can be decomposed to a sum (solid line) of two color centers:

$$D = \sum_{i=1}^2 A_i e^{-\frac{(E-E_i)^2}{2\sigma_i^2}} \quad (9)$$

where  $E_i$ ,  $\sigma_i$  and  $A_i$  denote the energy, width and amplitude of the color center  $i$ , and  $E$  is photon energy. As seen from these figures, the fit with two centers of Gaussian shape (dashed lines) provides

a rather good description of the radiation induced color center data with good  $\chi^2/\text{DoF}$ .

Table 5 lists fit result of radiation induced color centers for seven samples listed in Table 4. It is interesting to note that all these samples have a common center peaked at wavelength of 353 nm (3.51 eV) with a width from 0.25 to 0.54 eV. The other less energetic center, however, is peaked at 537 nm (2.31 eV) for samples prepared without oxygen compensation and 425 nm (2.92 eV) for samples with oxygen compensation. These centers are deeper than radiation induced color centers (3.07 and 2.30 eV) in trivalent doped samples [16], indicating a slower recovery speed, or a higher stability in situ.

### 3.5. Radiation hardness

The most direct representation of crystal radiation hardness is the degradation of its light output after irradiation. We use light output normalized to that before irradiation to represent crystal's radiation resistance. To reduce uncertainties of the measurement, light output was defined by an average of several measurements with a collimated  $^{137}\text{Cs}$  source shooting at evenly distributed positions along the sample. We used 9 measurements for CMS size samples and 5 measurements for samples of 10 cm.

Figs. 13 and 14 show light output degradation (solid dots with error bars) as a function of time under irradiation for four small and three large samples, respectively. Measurements were made

step by step for two different dose rates: 15 and 500 rad/h, as shown in these figures. The dose rate dependence of light output degradation and the improvement of radiation hardness by oxygen compensation are clearly observed. It is interesting to note that the radiation damage in Sb doped samples is less dose rate dependent than La doped samples [4]. This is consistent with the fact that Sb doped sample has deeper radiation induced color centers as compared to that of trivalent doped

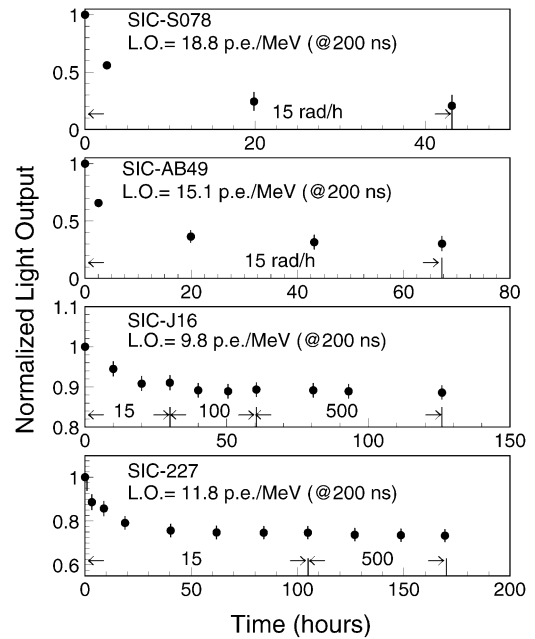


Fig. 13. Normalized light output as a function of time after irradiation for four small  $\text{PbWO}_4$  crystals.

Table 5  
Radiation induced color centers

ID	$E_1$ (eV)	$\sigma_1$ (eV)	$A_1^a$ (1/m)	$A_1^b$ (1/m)	$E_2$ (eV)	$\sigma_2$ (eV)	$A_2^a$ (1/m)	$A_2^b$ (1/m)
AB49	2.31	0.40	3.72	3.80	3.51	0.54	5.87	6.43
S078	2.31	0.55	4.58	5.50	3.51	0.44	7.96	8.76
J16	2.92	0.45	0.35	0.47	3.51	0.25	0.61	0.92
274	2.92	0.45	0.32	0.37	3.51	0.25	0.87	0.88
275	2.92	0.45	0.21	0.23	3.51	0.25	0.39	0.40
227	2.92	0.79	0.78	0.84	3.51	0.35	1.28	1.35
230	2.92	0.79	0.25	0.39	3.51	0.35	0.10	0.10

<sup>a</sup> Represents dose rate of 15 and 100 or 500 rad/h, respectively.

<sup>b</sup> Represents dose rate of 15 and 100 or 500 had/h, respectively.

Table 6  
Light output (%) in equilibrium under irradiation

R (rad/h)	S078	AB49	J16	227	230	274	275
15	20.7	31.6	91.0	74.8	84.1	82.0	83.6
500	—	—	88.9	73.4	79.0	78.0	80.0

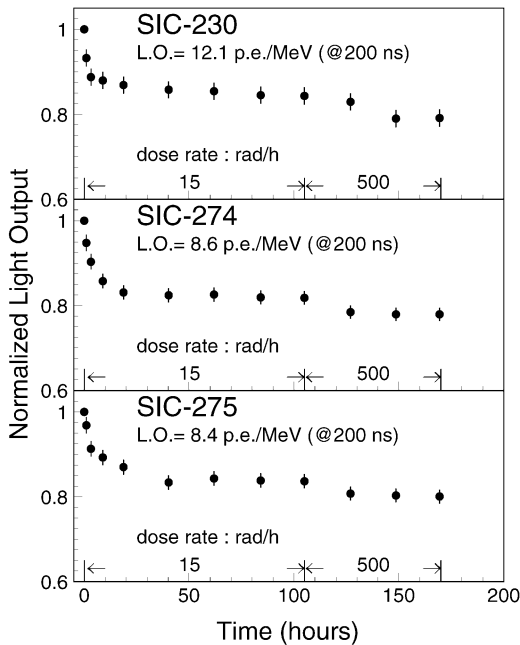


Fig. 14. Normalized light output as a function of time after irradiation for three large size  $\text{PbWO}_4$  crystals.

sample, as discussed in Section 3.4 above. The numerical result of this measurement is listed in Table 6.

#### 4. Summary

As compared to undoped  $\text{PbWO}_4$  crystal Sb doping is found to reduce slow scintillation components. Oxygen compensation is also found to have no effect on scintillation and decay kinetics for Sb doped  $\text{PbWO}_4$  crystals. The concentration of Sb ions in  $\text{PbWO}_4$  crystals is inhomogeneous. The segregation coefficient of Sb in  $\text{PbWO}_4$  crystals is determined to be  $0.052 \pm 0.004$ , indicat-

ing the difficulty of Sb ions to enter the  $\text{PbWO}_4$  lattice. A broad radio luminescence peaked at the blue (430–450 nm) was observed for Sb doped  $\text{PbWO}_4$  crystals, and it has a 50–60 nm blue shift as compared to that of photo luminescence. This shift is explained by not energetic enough photons of the UV excitation light.

The radiation induced absorption in all samples can be decomposed to two color centers with a common center peaked at wavelength of 353 nm (3.51 eV) of a width from 0.25–0.54 eV. The other less energetic center, however, is peaked at 537 nm (2.31 eV) for samples prepared without oxygen compensation and 425 nm (2.92 eV) for samples prepared with oxygen compensation. These centers are deeper than radiation induced color centers in trivalent doped samples (3.07 and 2.30 eV) [16]. This explains a smaller dose rate dependence of radiation damage in Sb doped  $\text{PbWO}_4$  crystals.

The Sb doping alone is found not improving crystal radiation hardness. Oxygen compensation is required to make Sb doped crystals radiation hard. Because Sb ions function as pentavalent in high temperature, Sb doping does not make effective compensation for the intrinsic oxygen vacancies in  $\text{PbWO}_4$  crystals. A more effective compensation of oxygen vacancies is achieved by trivalent doping, such as Y, which will be discussed in another paper. Results consistent to what presented here were also reported by Chen et al. [17].

#### Acknowledgements

Prof. D.Z. Shen and G.Q. Hu provided part of samples in this report. Part of the GDMS data used in this report was provided by

Dr. P. Lecomte. Many interesting discussions with Drs. H.F. Chen G.Q. Hu, M. Kobayashi, P. Lecomte, F. Nessi, D.Z. Shen and D.S. Yan are acknowledged. This work is supported in part by U.S. Department of Energy Grant No. DE-FG03-92-ER40701.

## References

- [1] Compact Muon Solenoid Technical Proposal, CERN/LHCC 94-38. LHCC/P1, 1994.
- [2] The CMS Electromagnetic Calorimeter Project, CERN/LHCC 97-33, 1997.
- [3] R.Y. Zhu et al., Nucl. Instr. and Meth. A 376 (1996) 319.
- [4] R.Y. Zhu et al., IEEE Trans. Nucl. Sci. NS-45 (1998) 686.
- [5] A.N. Annenkov et al., CMS NOTE, 1997/055.
- [6] M. Nikl et al., J. Appl. Phys. Lett. 82 (1997) 5758.
- [7] R.Y. Zhu, IEEE Trans. Nucl. Sci. NS-44 (1997) 468.
- [8] Z.Y. Wei et al., Nucl. Instr. and Meth. A 297 (1990) 163.
- [9] P. Lecoq et al., Nucl. Instr. and Meth. A 365 (1995) 291.
- [10] M. Kobayashi et al., Nucl. Instr. and Meth. A 399 (1997) 261.
- [11] M. Kobayashi et al., Nucl. Instr. and Meth. A 404 (1998) 109.
- [12] S. Baccaro et al., Phys. Stat. Sol. A 164 (1997) R9.
- [13] E. Auffray et al., Nucl. Instr. and Meth. A 402 (1998) 75.
- [14] Z.W. Yin, et al., Proceedings of SCINT99, Moscow, 1999.
- [15] M. Kobayashi et al., Nucl. Instr. and Meth. A 373 (1996) 333.
- [16] X.D. Qu et al., IEEE Trans. Nucl. Sci. NS-47 (2000) 1741.
- [17] H.F. Chen et al., Proceedings of SCINT99, Moscow, 1999.